Development 138, 203-213 (2011) doi:10.1242/dev.054916

Impaired mesenchymal stem cell differentiation and osteoclastogenesis in mice deficient for *Igf2-P2* transcripts

Sylvie Nathalie Hardouin[1,2,3,*], Ruolin Guo[4], Paul-Henri Romeo[1,2], Andras Nagy[3,4] and Jane E. Aubin[4]

SUMMARY

During embryonic development, *Igf2* gene transcription is highly regulated through the use of several promoters whose specific roles are not defined. Here, we show that loss-of-function of one of these promoters, *Igf2-P2*, results in growth defects that are temporally and quantitatively different from those seen in *Igf2*-null mutants. In particular, *Igf2-P2* mutants exhibit skeletal abnormalities characterized by thin and short bones with reduced mineralization and medullar cavity and with altered bone remodeling. These abnormalities are associated with decreased numbers of embryonic mesenchymal chondroprogenitors, adult mesenchymal stem cells and osteoprogenitors. Differentiation of osteoprogenitors into osteoblasts is impaired in the *Igf2-P2* mutant mice in a cell-autonomous manner, and osteopontin is a target of the IGF2 signaling pathway during this differentiation. *Igf2-P2* mutant mice also display impaired formation of giant osteoclasts owing to a defective micro-environment. These results support a model wherein transcriptional activity of the *Igf2-P2* promoter regulates the fate of mesenchymal progenitors during bone development and remodeling in the adult, and regulates osteogenesis in a cell-autonomous and non-autonomous manner.

KEY WORDS: Igf2, Osteogenesis, Progenitors, Mesenchymal stem cells, Stromal environment, Mouse

INTRODUCTION

IGF (insulin-like growth factor)/insulin is a major signaling pathway, highly conserved throughout evolution, that regulates cell proliferation, differentiation, aging and life span. In lower organisms, it regulates progression either to active proliferation or quiescence, acts as the major growth-promoting system that controls body size and orchestrates the complex interactions that determine the size of an organism (Conlon and Raff, 1999; Weinkove and Leevers, 2000). The IGF signaling pathway is activated after binding of IGF1 or IGF2 to IGF Type I receptor (IGF-R), insulin-receptor (Ins-R) and IGF/insulin hybrid-receptor, and acts locally as an extremely potent mitogen, ensuring proliferative, anti-apoptotic and metabolic roles (Federici et al., 1997; Belfiore et al., 2009).

In mouse, IGF2 is thought to act only during development, whereas IGF1 also acts after weaning and in the adult. *Igf2* transcripts can be detected as early as the two-cell stage embryo, and are then found in all components of the chorio-allantoic placenta (Lee et al., 1990) and in most tissues derived from the somites and the lateral plate of the embryo proper, but not in the ectoderm-derived central and peripheral nervous system (Stylianopoulou et al., 1988). The *Igf2* gene is not transcribed in most tissues after weaning and, in adult mice, expression of the *Igf2* gene has been detected only in the choroids plexus and the leptomeninges (DeChiara et al., 1991). Interestingly, although the role of IGF2 during embryonic development is well known, its expression in minority adult cell populations such as stem cells and its possible function(s) after birth have not been studied, even though somatic stem cells arise in the embryo at specific stages of organ formation when IGF2 is crucial for development.

The *Igf2* gene displays a parental imprint and is expressed only from the paternal allele. Deregulation of the *Igf2* gene parental imprint results in expression from maternal and paternal alleles, leads to loss of imprinting (LOI) and IGF2 overexpression. LOI of the *Igf2* gene occurs in a genetic human disease, Beckwith Wiedeman Syndrome, which is characterized by an organomegaly and tumor predisposition (Ping et al., 1989). By contrast, in humans, underexpression of IGF2 is associated with the Silver Russel Syndrome, which is characterized by a small size at birth owing to developmental defects (Gicquel et al., 2005). Finally, in mouse and human, numerous tumor cells express the *Igf2* gene bi-allelically (Cui, 2007; Randhawa et al., 1998; Hattori et al., 2000; Vorwerk et al., 2003), suggesting that increased level of IGF2 might be involved in cancer progression.

In human and mouse, the *Igf2* gene uses four alternative promoters (P0 to P3 in mouse) for its developmentally and epigenetically regulated expression. Except for the mouse P0 promoter, which is placental specific (Constância et al., 2002), the specific roles of the other promoters have not been deciphered (DeChiara et al., 1990). Transcripts initiated from the P2 promoter have the broadest expression in developing mouse embryo, are often expressed from the maternal and paternal alleles in mouse and human cancer cells and in hematopoietic progenitors (Vorwerk et al., 2003; Morison et al., 2000; Hofmann et al., 2002), whereas only the paternal P2 promoter is active in differentiated hematopoietic cells (Morison et al., 2000). These results suggest that *Igf2-P2* may play a role at very early stages of embryonic development in determining the size of progenitor pools, then acts postnatally to regulate the survival of these pools in their interactions with the stem cell niches. To test these hypotheses, we replaced the P2 driven transcriptional unit of the *Igf2* gene with a *lacZ-Neo* cassette in ES cells. Here, we show that mutant mice

[1]INSERM UMR 967, Fontenay-aux-Roses, F-92265, France. [2]CEA, DSV-Institut de Radiobiologie Cellulaire et Moleculaire (IRCM), Laboratoire de Recherche sur la Reparation et la Transcription dans les Cellules Souches (LRTS), Fontenay-aux-Roses, F-92265, France. [3]Samuel Lunenfeld Research Institute, Mount Sinai Hospital, Toronto, Ontario, M5G 1X5, Canada. [4]Department of Molecular Genetics, University of Toronto, Ontario M5S 1A8, Canada.

*Author for correspondence (sylvie.hardouin@cea.fr)

Accepted 11 November 2010

derived from these targeted ES cells are viable and fertile but exhibit growth retardation and skeleton abnormalities linked to impaired IGF2 functions in embryonic and adult mesenchymal progenitors and during osteoclastogenesis.

MATERIALS AND METHODS

Construction of the *Igf2-P2* targeting vector and genotyping of the offspring

Two *Igf2* mouse genomic DNA probes were used to screen a 129 Sv/J mouse genomic lambda FIXII phage library (Stratagene). One clone spanning 18 kb of genomic sequence starting upstream of exon 1, was selected and cut into three restriction fragments with *Xho*I. A *lacZ-Neo-pA* cassette was inserted into the middle *Xho*I restriction fragment to replace exon 2. This fragment was inserted into the *Xho*I site flanked by a short 5′ arm and a long 3′ arm of *Igf2* homology (see Fig. S1A in the supplementary material). Mouse ES cells R1 (Nagy et al., 1993) were electroporated with the *Igf2* targeting vector and screened for the insertion of the targeting vector using geneticin (G418, Invitrogen). Genomic DNA extracted from G418r clones was cut with *Eco*RV and analyzed by Southern blot hybridization (see Fig. S1B in the supplementary material). Targeted ES clones were used to create chimeras that were crossed with wild-type ICR females. Offspring were genotyped by PCR with *lacZ* primers: forward, 5′-GCT CAT GCT ATG GGC AAC AGC-3′; reverse, 5′-TGG ATG AGG TGT CCT GTC AGC-3′.

Animal care and breeding procedures

Animals were generated and analyzed in the Toronto Center for Phenogenomics (TCP). Experimentation was conducted in accordance with the Canadian Guide for the Care and Use of Laboratory Animals and approved by the Animal Care Committee at TCP. For growth curves, timed matings were performed taking the morning of vaginal plug as day 0.5, then body weight was measured daily from E9.5 up to 37 days postnatally, then until the ninth week.

Body composition analysis, high-resolution μCT and histology

Body composition and bone mineral density (BMD: g/cm^2) were analyzed using a PIXImus Small Animal Densitometer (Lunar, Madison, WI, USA). Analyses were carried out on wild-type and *Igf2-P2* mutant littermates at 8 and 12 weeks, then on 1-year-old mice. High-resolution μCT (micro-computed tomography in vivo imaging, μCT 40, Scanco Medical, Wayne, PA, USA) was used for three-dimensional reconstruction and quantification of bone parameters of 3-month-old mice. Limbs from 3- and 12-month-old mice were used for histology. Entire skeletons of E14.5 to E18.5 fetuses were visualized with Alcian Blue and Alizarin Red.

Ex vivo osteoblast and osteoclast differentiation assays

Osteoblast and osteoclast differentiation assays were performed as described previously (Malaval et al., 2008). For osteoblast differentiation assay, bone marrow cells were flushed from femurs and tibias of 2- to 4-month-old wild-type and *Igf2-P2* mutant mouse littermates, in α-minimum essential medium containing 15% FCS and antibiotics (100 μg/ml penicillin G and 50 μg/ml gentamycin from Sigma-Aldrich, 300 ng/ml fungizone from Flow Laboratories) then cells were filtered using a 70 μm mesh filter and treated with NH_4Cl to lyse and eliminate anucleated red blood cells. For stromal colony counts and osteoblast differentiation assays, 10^6 nucleated cells were plated into 35 mm dishes, cultured for 7 days at 37°C and 5% CO_2, then switched to osteogenic differentiation medium (medium as above containing 10% FCS, 50 μg/ml ascorbic acid and 10 mM β-glycerophosphate). Staining and quantification of colony types and numbers were performed at day 0, 7 and 14 of differentiation.

The osteoclast differentiation assay was performed with nucleated cells from bone marrow and spleens from 2- to 4-month-old mice. Spleens were crushed, then cells were treated like bone marrow cells (cf supra). Nucleated cells were plated into 96-well plates at 10^5 cells/well, grown in α-minimum essential medium containing 10% FCS, antibiotics, 50 ng/ml RANKL and 20 ng/ml MCSF (Peprotech) at 37°C and 5% CO_2. On day 7, cells were stained for TRAP activity at 37°C with 2 mg/ml Naphtol AS-TR Phosphate and 5 mg/ml Fast Violet B Salt (Sigma-Aldrich).

Osteoclasts in co-culture were generated from 3×10^4 calvaria cells of 3-day-old newborns and 1×10^5 splenic cells from 3- to 10-month-old mice per well of 96-well plates, in the presence of 10 nM 1,25-dihydroxyvitamin D3 (Sigma-Aldrich) for 7 days.

Ex vivo chondrogenic differentiation-micromass assay

Fore- and hindlimb buds from E11.5 wild-type and *Igf2-P2* mutant littermates were dissected and rinsed in PBS, placed in 0.2 ml Puck's saline solution containing 10% chicken serum and 0.2 ml of 0.1% dispase, at 37°C and 5% CO_2, until a single cell suspension was obtained. Primary cells were filtered, rinsed then 10^5 cells/10 μl were plated into 24-well plates and, after cell adhesion, 0.5 ml of DMEM-high glucose containing 10% fetal calf serum, antibiotics, 10 mM β-glycerol phosphate and 50 μg/ml ascorbic acid was added to induce chondrogenic differentiation. After 5 to 10 days, cells were stained with Alcian Blue and alkaline phosphatase.

Bone marrow transplantation

Igf2-P2 mutant mice backcrossed onto a 129 genetic background, and 129 mice expressing YFP transgene and used as wild type, were 2-4 months old. Nucleated cells (2.5×10^6) prepared from whole bone marrow flushed from two to four femurs and tibias of donors, were injected per recipient into the tail vein under sterile conditions. Recipient mice (n=3-7) were lethally irradiated with 9.5 Gy (1 Gy/minute) of total body irradiation from a ^{137}Cs source 4 hours before transplantation. Engrafted mice were maintained under SPF conditions in isolators and antibiotics were administrated for at least 2 weeks, with daily health checking. The transplanted mice were analyzed 5 months later.

Western blot, RT-PCR and real-time PCR

Western blot analyses were performed with total proteins extracted from whole embryos homogenized in RIPA buffer. Samples were applied to SDS-polyacrylamide gels (15%), proteins were transferred onto nitrocellulose membranes (Biorad) that were blocked in gelatin and incubated at 4°C overnight with an antibody to IGF2 (Abcam ab9574).

Total RNA was isolated from femoral cortical bones after they had been flushed to remove bone marrow cells, from spleens and from cultured bone marrow stromal cells (BMSCs), using TRIzol (Invitrogen), then reverse transcribed using the quantiTect Reverse Transcription kit (Qiagen). The iTaq SYBR Green Supermix (BioRad) and the 7300 Applied real time PCR detection system were used for real-time PCR, with the primers listed in Table S1 in the supplementary material. Relative expression was calculated for each gene by the 2-CT method with β-actin for normalization.

Statistical analysis

Data are plotted as mean ± s.e.m.; n is indicated in figure legends. Statistical analyses were performed using Student's t-test. A P-value of less than 0.05 was considered to be statistically significant.

RESULTS

Loss-of-function of *Igf2-P2* results in dwarf mice upon paternal transmission of the mutation

To target *Igf2-P2* promoter, E2 exon of the *Igf2* gene was replaced by a *lacZ-Neo* cassette in ES cells (see Fig. S1A in the supplementary material) and mice with homologous recombination were generated (see Fig. S1B in the supplementary material). Wild-type and mutant embryos were obtained with a Mendelian ratio but paternal transmission of the *Igf2-P2* mutated allele led to heterozygote (p–/m+) offspring exhibiting a phenotype, whereas maternal transmission of the mutation (p+/m–) led to offspring without phenotype. As a consequence, homozygote mice were similar to p–/m+ mice, and only p–/m+ and their wild-type littermates were analyzed. In mutant mice, the *lacZ-Neo* cassette was under the transcriptional control of the P2 promoter and this mutation resulted in a 40% decrease of total *Igf2* transcripts during development (Fig. 1A, left panel). The insertion of the *lacZ-Neo*

cassette under the transcriptional activity of the P2 promoter had an effect on the transcriptional activity of the adjacent P3 promoter during intra-uterine development, as shown by a 40% decrease of transcripts initiated from the P3 promoter in E11.5 mutants, followed by a 40% increase in activity of this promoter after mid gestation (Fig. 1A, right panel). There was no statistically significant difference in the expression of transcripts initiated from the *Igf2-P1* and *Igf2-P3* promoters in various tissues of 3-day-old pups compared with wild-type levels (not shown). Finally, as expected, no *Igf2* expression was detected in tissues of wild-type or mutant adult mice (not shown). IGF2 protein levels in whole mutant and wild-type littermate fetuses at different stages of development seemed unaffected in mutants compared with their wild-type littermates (Fig. 1B), indicating that the phenotypes observed might be due to decreased levels of IGF2 protein in discrete cell populations that could not be detected with the method used to quantify total IGF2 protein level.

At birth, heterozygote *Igf2-P2* (p–/m+) mutant mice exhibited growth retardation, and their body weight was 30% lower than that of wild-type littermates. At 12 weeks of age, all mutant mice were still growth retarded and this deficit remained constant throughout life (Fig. 1C, left panel; see Fig. S2A in the supplementary material). This growth retardation was similar to the one observed in *Igf2*-null mutants, but the phenotypes of the two mutants were different (Fig. 1C, right panel). To study the effect of the *Igf2-P2* loss-of-function on embryonic development, staged progeny from a male chimera and a wild-type female were analyzed from E10.5 to E18.5 of development using total body weight as phenotypic

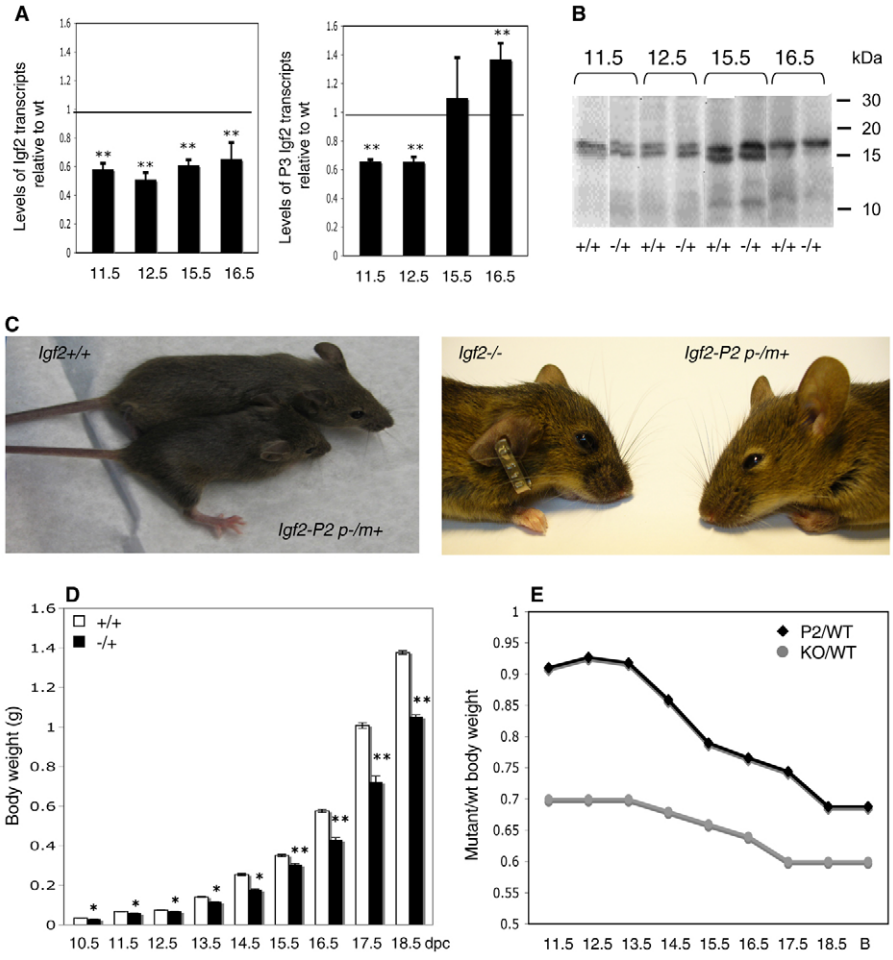

Fig. 1. Embryonic and postnatal growth defects of *Igf2-P2* mutant mice. (**A**) Real-time PCR analysis of *Igf2* transcripts in E11.5 to E16.5 mutant embryos. The left-hand panel shows the relative expression of *Igf2* transcripts initiated from all the *Igf2* gene promoters in mutant fetuses and the right-hand panel shows the relative expression of *Igf2* transcripts initiated from the P3 promoter in mutant fetuses. The expression level of total or of P3 specific *Igf2* transcripts in wild-type littermates is represented with a value of 1. Values are the mean ± s.e.m. of four embryos and fetuses for each day; ***P*<0.005. (**B**) Western blotting of IGF2 protein in total protein extracts from E11.5, E12.5, E15.5 and E16.5 wild-type and *Igf2-P2* mutant littermate fetuses. Two major signals were detected at 17 and 15 kDa. In mammals, high molecular weight forms of IGF2 correspond to precursor forms. They are known to be potent mitogens and better activators of the IGF type I receptor than is the fully processed form of IGF2 (Valenzano et al., 1998; Blahovec et al., 2001). To standardize the results, the same amounts of total proteins were used for all samples and the western membranes were stained with Ponceau Red. The experiments were carried out three times with the same results. (**C**) Left photo: growth defect of a 3-month-old *Igf2-P2* mutant mouse compared with a wild-type littermate. Right photo: phenotypic differences between 3-month-old *Igf2*-null and *Igf2-P2* mutant mice. (**D**) Growth curves of wild-type and *Igf2-P2* mutant embryos and fetuses. Values are the mean ± s.e.m of 12-16 embryos and fetuses for each day; **P*<0.01, ***P*<0.005. (**E**) Comparison of growth curves of *Igf2-P2* mutant and *Igf2*-null embryos. Ratios of *Igf2-P2* mutant embryo (black diamonds) and *Igf2*-null embryo (grey circles) [reproduced, with permission, from Baker et al. (Baker et al., 1993)] body weights to wild-type embryo body weights from E11.5 to birth.

criterion. Growth retardation could be detected as early as E10.5 in mutant embryos that were already 10% lighter than their wild-type littermates (Fig. 1D). Between E11.5 and E13.5, this 10% weight deficit remained stable and then gradually increased between E13.5 and E18.5, where a 30% weight deficit was observed, a deficit that thereafter remained unchanged over the entire life (Fig. 1E, black curve). This biphasic growth curve of *Igf2-P2* mutants contrasted with the growth curve of *Igf2*-null mutants (Fig. 1E, grey curve) that showed a rapid 30% lower body weight than wild-type littermates between E10.5 and E11.5 followed by a gradual decrease to 40% between E13.5 and E17.5 (Baker et al., 1993). Taken together, these results indicated that the phenotype of the *Igf2-P2* mutant mice was related but different from the *Igf2*-null mutant phenotype.

Igf2-P2 transcriptional activity regulates the number of embryonic mesenchymal chondroprogenitors and adult mesenchymal stem cells (MSCs), and the number and potential of adult osteoprogenitors

From E14.5 into adulthood, a striking feature of *Igf2-P2* mutant mice was a skeletal defect characterized by delayed ossification and thinner and shorter bones (Fig. 2A). Bone mineral density was significantly decreased in 2-month-old mutants compared with their wild-type littermates, with the same deficit still seen in 3-month-old mutants, i.e. when growth has largely ended in wild type (Fig. 2B) and in 1-year-old mice (see Fig. S2B in the supplementary material). In 3- to 4-month-old *Igf2-P2* mutant mice, bones were thinner than in wild-type littermates and poorly

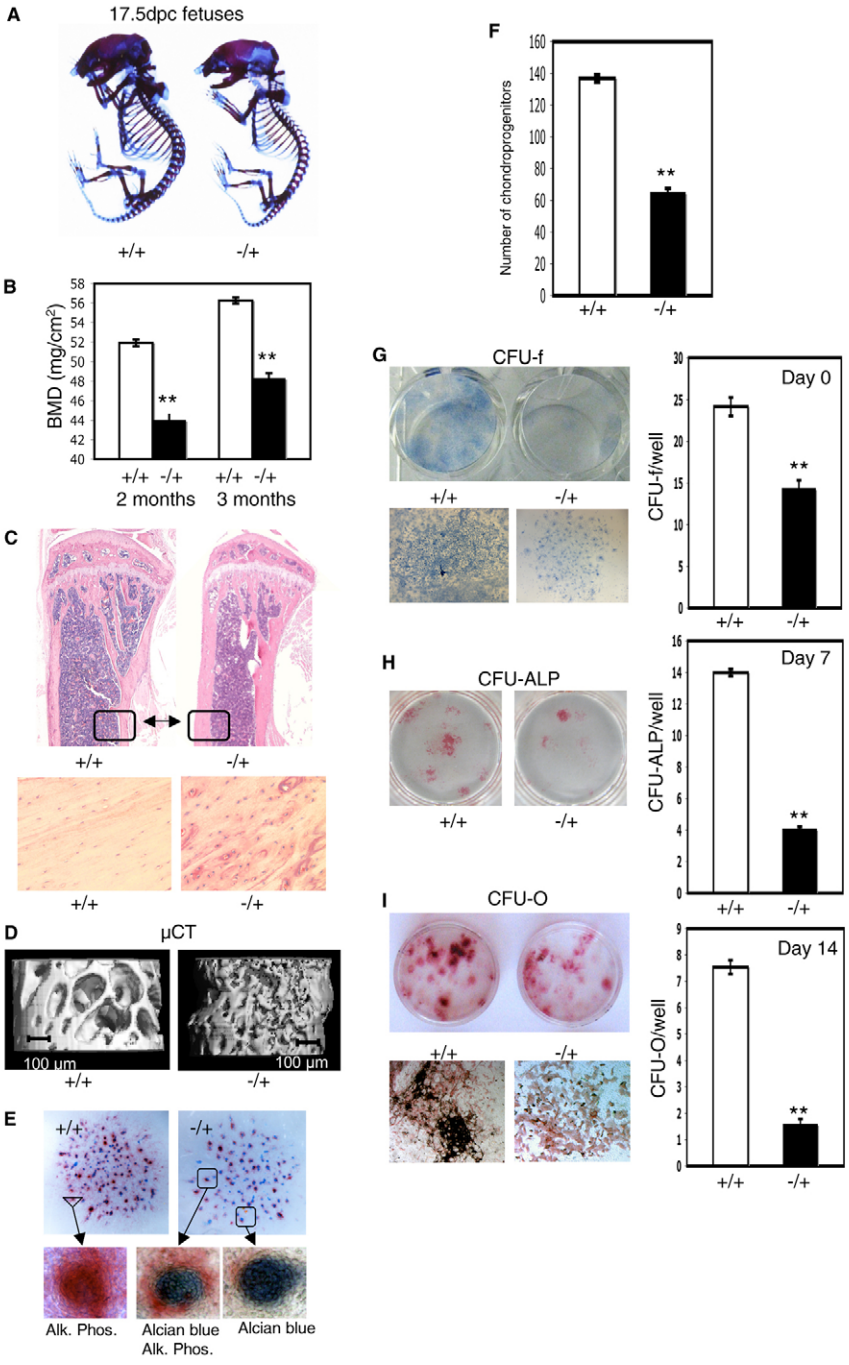

Fig. 2. *Igf2-P2* transcripts regulate the number of embryonic chondroprogenitors, the number of adult MSCs and the differentiation potential of adult osteoprogenitors. (**A**) Skeletal preparations of E17.5 wild-type (+/+) and *Igf2-P2* mutant (–/+) fetuses stained with Alcian Blue and Alizarin Red. (**B**) Bone mineral density of adult wild-type (+/+) (n=12) and *Igf2-P2* mutant (–/+) (n=12) littermates. $^{**}P<0.05$. (**C**) Upper panels: Hematoxylin and Eosin staining of longitudinal sections of tibias of 3-month-old mice; black boxes indicate the locations of higher magnifications of cortical bone in wild-type (+/+) or *Igf2-P2* mutant (–/+) mice shown in the lower panels. (**D**) X-ray microcomputed tomography (µCT) was used to allow a three-dimensional image reconstruction of epiphyseal trabecular bone in 3-month-old wild-type (+/+) and *Igf2-P2* mutant (–/+) littermates. (**E**) Ex vivo chondroprogenitor colonies in E11.5 limb bud cell micromass cultures of wild-type (+/+) and *Igf2-P2* mutant (–/+) littermates. Lower panels: higher magnification of mature differentiated (alkaline phosphatase) and more immature (Alcian Blue) chondrocyte colonies in wild-type (+/+) and *Igf2-P2* mutant (–/+) cell cultures. (**F**) Number of chondroprogenitor colonies from wild-type (+/+) and *Igf2-P2* mutant (–/+) cells per well. Five to 14 wells were analyzed (n=4 independent experiments). $^{**}P<0.005$. (G-I) Osteoblastic differentiation of cells from wild-type and *Igf2-P2* mutant bone marrow stromal cell cultures. (**G**) Representative pictures of mesenchymal stem cells (CFU-f; methylene blue-positive) (left upper panel) and number of total CFU-f (right panel) in wild type and *Igf2-P2* mutants. Lower left panels: high magnification of typical CFU-f in wild type and *Igf2-P2* mutants; $^{**}P<0.005$. (**H**) Representative pictures of osteoprogenitors (CFU-ALP; no mineralized matrix) (left panel) and the number of CFU-ALP (right panel) in wild-type and *Igf2-P2* mutant cell cultures; $^{**}P<0.005$. (**I**) Representative pictures of mature osteoblasts colonies (CFU-O; ALP-positive cells and mineralized matrix) (upper left panel) and number of CFU-O (right panel) in wild-type and *Igf2-P2* mutant cell cultures. Lower left panels: high magnification of individual wild-type and *Igf2-P2* mutant colonies. Eight to 16 wells analyzed (n=5 independent experiments). $^{**}P<0.005$. Statistical analysis was performed using a two-tailed t-test. Error bars indicate s.e.m.

mineralized, but without any other obvious or gross abnormalities (data not shown). Histological analysis of longitudinal tibia sections revealed that, although the bones were thinner, cortical bone was thicker and marrow cavity was reduced in the mutant mice (Fig. 2C, upper panel) and this defect was still present in bones of 1-year-old *Igf2-P2* mutant mice (see Fig. S2C in the supplementary material) where mutant bones still contained fewer trabeculae. At higher magnification, the lamellar structure of the cortical bone was irregular and poorly formed, with poorly aligned osteocytes and incompletely formed lacunae (Fig. 2C, lower panel). High-resolution μCT of femurs revealed dense and disorganized trabeculae in bones of 3-month-old mutant versus wild-type mice (Fig. 2D). Thus, the *Igf2-P2* mutation led to smaller bones with increased but poorly organized and poorly mineralized cortical and trabecular bone, and a reduced medullar cavity, suggesting defects in both osteoblasts and osteoclasts functions.

We next determined whether there was any difference in embryonic mesenchymal cells and in chondroprogenitors. The number of chondrocyte colonies formed in E11.5 *Igf2-P2* mutant limb bud mesenchymal cell cultures was decreased to ~60% that of wild type; chondrocyte colonies that formed did so more slowly (i.e. day 3 versus day 2 of micromass culture) and had a less mature phenotype than did wild-type colonies (Fig. 2E,F). Interestingly, this 40% decrease in embryonic chondroprogenitors was observed in cells collected from E11.5 limb buds, i.e. when the weight deficiency of mutant embryos was reduced by only 10% of wild-type body weight, indicating that, in early embryos, the *Igf2-P2* promoter is necessary for the establishment and maintenance of embryonic chondroprogenitors.

To determine whether the deficit in skeletal progenitor cells was observed also after birth, we quantified the MSC and osteoprogenitor populations in adult mice. Ex vivo differentiation of bone marrow stromal cells from 3- to 4-month-old mice revealed approximately half the number of MSCs (i.e. CFU-f) (Fig. 2G, upper and right panels), ~30% of the osteoprogenitors (CFU-ALP with unmineralized matrix) (Fig. 2H) and ~20% of the mature osteoblast colonies (CFU-O with ALP-positive cells and mineralized matrix) (Fig. 2I, upper and right panels) in *Igf2-P2* mutant versus their wild-type littermates. In addition, most of the CFU-f, CFU-ALP and CFU-O colonies obtained from mutant mice were smaller and contained cells with fewer contacts and less dense packing than wild-type colonies (lower panels in Fig. 2G,I). These results indicated that the *Igf2-P2* mutation also affected the number or capacity of adult bone marrow MSC/mesenchymal progenitors to form colonies and mature osteoblasts.

The IGF2 signaling pathway regulates the differentiation of mesenchymal progenitors into osteoblasts

Consistent with the results obtained using colony formation endpoints, mRNA levels of two crucial transcriptional activators of the osteoblast lineage, RUNX2 and osterix (*Osx*), were markedly decreased in femoral bones of 3-month-old *Igf2-P2* mutant versus wild-type bones (Fig. 3A). The lower expression of OSX compared with RUNX2 is in agreement with RUNX2 being a transactivator of the *Osx* gene (Nishio et al., 2006). Furthermore, RUNX2 and OSX mRNA levels were decreased in MSC (OSX) and osteoprogenitors (RUNX2 and OSX) obtained under osteogenic differentiation conditions (Fig. 3B, left and middle panels) but the rates of induction of RUNX2 and OSX mRNAs were similar when MSC from 3-month-old *Igf2-P2* mutant or wild-type mice underwent osteogenic differentiation (Fig. 3B, right panel).

Quantification of the mRNA levels of several markers of osteoblasts in femoral bones showed that only osteopontin (OPN) mRNA level was significantly decreased (Fig. 3C). Using ex vivo osteogenic differentiation of MSC, we showed that bone sialoprotein (BSP), type I collagen (COL1) and alkaline phosphatase (ALP) mRNA had a kinetics of expression that paralleled the RUNX2 or OSX kinetics (Fig. 3D), whereas OPN mRNA levels were similar in MSC from 3-month-old *Igf2-P2* mutant versus wild-type mice but were not increased during osteogenic differentiation of the *Igf2-P2* mutant derived MSC (Fig. 3D). The decrease in markers of not only mature osteoblasts but also osteoprogenitors (i.e. RUNX2), together with colony formation results indicated that the *Igf2-P2* mutation has a very early effect on MSC/osteoprogenitor cells.

Taken together, these results indicated that *Igf2-P2* transcriptional activity regulated: (1) the number of MSC in adult mice, as well as their subsequent commitment towards the osteoblast lineage by regulating the level of osteoblast-specific transcription factors such as OSX in MSC; and (2) the differentiation of osteoblastic progenitors, as well as the function of the mature osteoblasts, by modulating the levels of the extracellular matrix protein OPN, which is known to be involved in osteoblasts differentiation as well as in cell migration and adhesion (Liaw et al., 1995).

Osteoclastogenesis is impaired in *Igf2-P2* mutant mice owing to a stromal cell deficiency and an intrinsic osteoclast defect

The reduced marrow cavity, together with the osteoblast deficiency in *Igf2-P2* mutant mice suggested that osteoclastogenesis might also be impaired in mutant animals. Wild-type and *Igf2-P2* mutant hematopoietic progenitors from the bone marrow (Fig. 4A-C) or spleen (Fig. 4D-F) of 3- to 4-month-old mice cultured with macrophage colony-stimulating factor (M-CSF) and receptor activator of NF-κB ligand (RANKL) gave rise to similar numbers of mononucleated and medium-sized TRAP-positive osteoclasts (Fig. 4A; Fig. 4D, one nucleus), but mutant cells formed fewer large (more than 10 nuclei for bone marrow and more than two nuclei for spleen) osteoclasts (Fig. 4B,C, for bone marrow; Fig. 4D-F, for spleen). As peroxisome proliferator-activated receptor γ (PPARγ) regulates osteoclast differentiation (Wan et al., 2007), we determined PPARγ mRNA levels in femurs of 3- to 4-month-old mice and found an 80% reduction in *Igf2-P2* mutant versus wild-type femurs (Fig. 4G). RANKL mRNA level was threefold higher in the mutant femurs, whereas the mRNA level of osteoprotegerin (OPG), a decoy receptor for RANKL, was not affected (Fig. 4G), indicating a possible compensatory response to the low levels of PPARγ mRNA.

To address the cell-autonomous and/or cell non-autonomous basis for the impaired ability of *Igf2-P2* mutant monocytes-macrophages to form mature multinucleated osteoclasts, wild-type bone marrow cells from mice carrying a ubiquitously expressed YFP transgene (YFP^+) were transplanted into lethally irradiated *Igf2-P2* mutant mice or, reciprocally, *Igf2-P2* mutant bone marrow cells were transplanted into lethally irradiated wild-type YFP^+ mice. Five months after bone marrow transplantation, the ability of engrafted monocytes-macrophages to differentiate ex vivo into small and/or large osteoclasts was analyzed. Osteoclasts derived from *Igf2-P2* mutant monocytes-macrophages engrafted into wild-type YFP^+ mice were able to form giant multinucleated cells, but osteoclasts derived from wild-type YFP^+ monocytes-macrophages engrafted into *Igf2-P2*

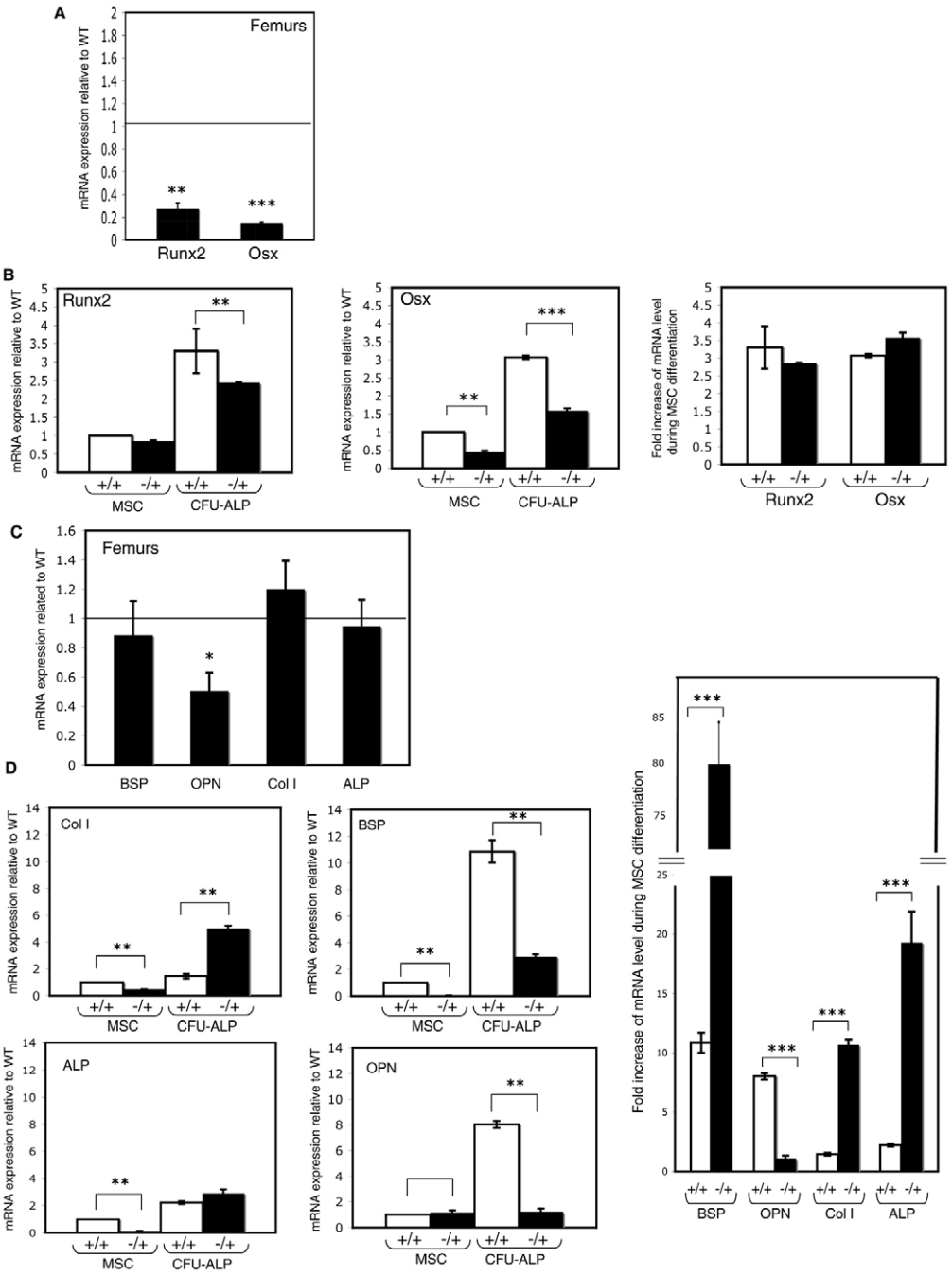

Fig. 3. *Igf2-P2* transcripts modulate the mRNA levels of osteoblast-specific transcription factors and extracellular matrix components in adult femurs, in mesenchymal stem cells and in osteoprogenitors. (**A**) Real-time PCR analysis of RUNX2 and osterix (OSX) mRNA levels in femurs of 3- to 4-month-old *Igf2-P2* mutant mice relative to wild type. RUNX2 and OSX mRNA levels in *Igf2-P2* mutants are shown as percentages of wild-type RUNX2 and OSX mRNA levels. Results are the mean ± s.e.m. of results obtained from three *Igf2-P2* mutant and three wild-type mice. Each sample was analyzed by q-PCR in triplicate and normalized to β-actin mRNA levels (RUNX2, $^{**}P<0.005$; OSX, $^{***}P<0.001$). (**B**) Left panels: real-time PCR analysis of RUNX2 (left panel) and OSX (middle panel) mRNAs levels in mesenchymal stem cells (MSCs) (day 0) and osteoprogenitors (CFU-ALP, day 7) from wild-type and *Igf2-P2* mutant mice. Right panel: fold increase in RUNX2 and OSX transcripts between day 0 and day 7 of MSC differentiation from wild-type or *Igf2-P2* mutant mice. Results are mean ± s.e.m. of results obtained from three *Igf2-P2* mutant and three wild-type bone marrow-derived MSCs. Each sample was analyzed by q-PCR in triplicate and normalized to β-actin mRNA levels (RUNX2, $^{**}P<0.05$; OSX, $^{***}P<0.001$). (**C**) Real-time PCR analysis of mRNA levels of bone sialoprotein (BSP), osteopontin (OPN), type I collagen (COL1) and tissue non-specific alkaline phosphatase (ALP) extracellular matrix proteins in femurs of 3- to 4-month-old *Igf2-P2* mutant mice relative to wild type. *Igf2-P2* BSP, OPN, COL1 and ALP mRNA levels are shown as percentages of wild-type BSP, OPN, COL1 and ALP mRNA levels. Results are the mean ± s.e.m. of results obtained from three *Igf2-P2* mutant and three wild-type mice. Each sample was analyzed by q-PCR in triplicate and normalized to β-actin mRNA levels (OPN, $^{*}P<0.05$). (**D**) Left panels: real-time PCR analysis of COL1, BSP, ALP and OPN mRNAs levels in MSCs (day 0) and osteoprogenitors (CFU-ALP, day 7) from wild-type and *Igf2-P2* mutant mice. Right panel: fold increase of BSP, OPN, COL1 and ALP transcripts between day 0 and day 7 of MSC differentiation from wild-type or *Igf2-P2* mutant mice ($^{**}P<0.001$). Results are the mean ± s.e.m. of results obtained from three *Igf2-P2* mutant and three wild-type bone marrow-derived MSCs. Each sample was analyzed by q-PCR in triplicate and normalized to β-actin mRNA levels ($^{***}P<0.005$).

mutant mice gave rise only to osteoclasts with fewer than 10 nuclei (Fig. 5A-C), which also confirmed that osteoclastogenesis is still defective in older mutant mice. Similar deficiency in the formation of giant multinucleated osteoclasts was obtained when splenic precursors were differentiated into osteoclasts but this deficiency was restricted to osteoclasts with more than 10 nuclei and the number of osteoclasts with one nucleus was significantly increased when wild-type YFP$^+$ bone marrow was transplanted into *Igf2-P2* mutant mice (Fig. 5D,E,F). The mRNA level of PPARγ was higher in the spleen of YFP$^+$ mice engrafted with *Igf2-P2* hematopoietic cells than in the spleen of *Igf2-P2* mutant mice engrafted with YFP$^+$ hematopoietic cells (Fig. 5G), indicating that the recipient wild-type YFP$^+$ micro-environment could rescue the ability of *Igf2-P2*-deficient monocytes-macrophages to differentiate into giant osteoclasts. Thus, the *Igf2-P2* mutation resulted in a micro-environment that impaired the capacity of monocytes-macrophages to give rise to osteoclasts that fuse into giant cells, but with different effects in bone marrow- and spleen-derived mononucleated osteoclasts.

To determine whether the defective osteoclastogenesis in *Igf2-P2* mutant mice was due to an impaired interaction between osteoblasts and osteoclasts, co-culture studies were performed using different combinations of osteoblastic cells derived from newborn calvaria (Fig. 6A) and splenic osteoclast precursors from wild-type and *Igf2-P2* mutant mice (Fig. 6B). When wild-type osteoblastic cells were used with mutant spleen cells, similar numbers of giant osteoclasts were obtained, suggesting that the defect in mutant osteoclasts could be rescued in a wild-type environment, thus confirming the results obtained from the bone marrow transplantation experiments. When *Igf2-P2* mutant osteoblastic cells were used with wild-type spleen cells, reduced numbers of giant osteoclasts were generated, also indicating that

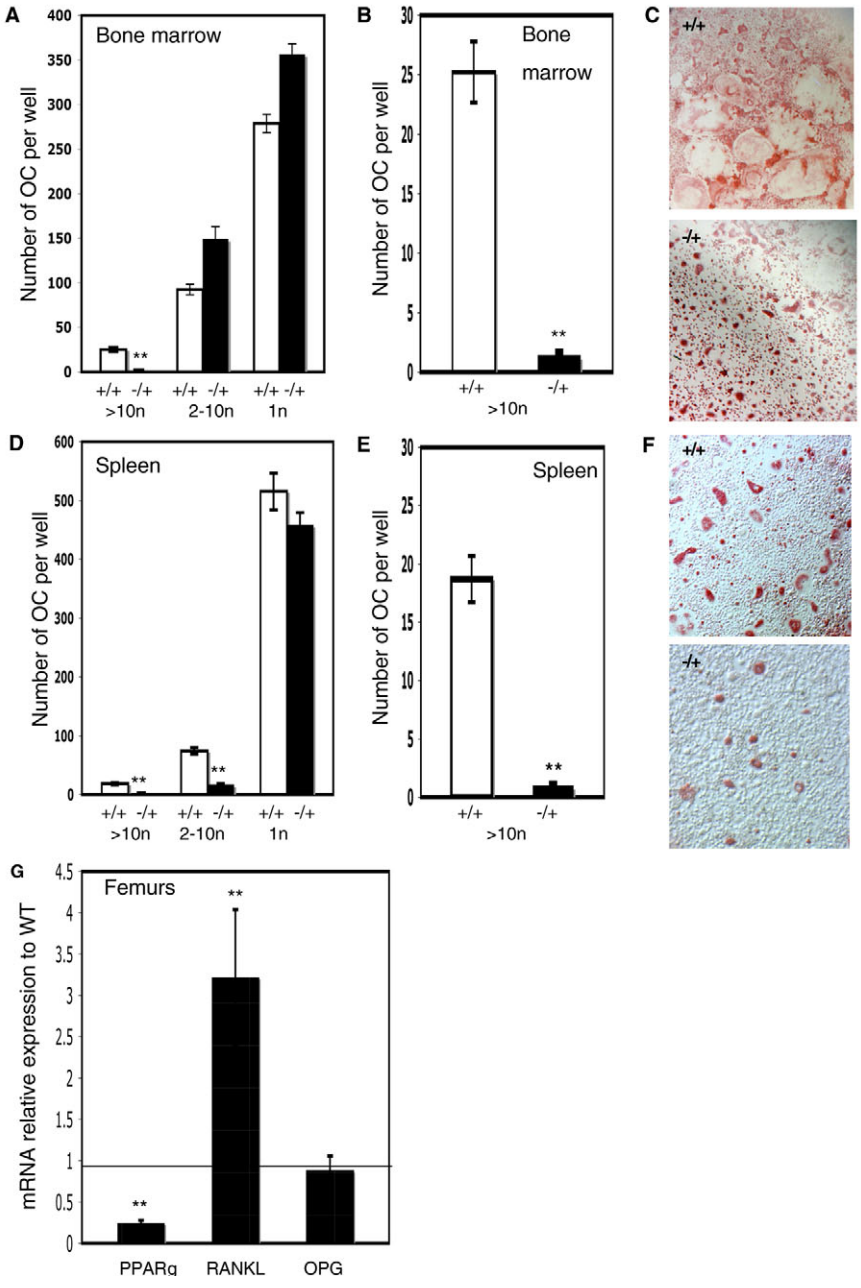

Fig. 4. Development of giant osteoclasts is impaired in *Igf2-P2* mutants. (**A**) Numbers of giant (>10 nuclei), medium-sized (2-10 nuclei) and mononucleated TRAP$^+$ osteoclasts obtained ex vivo from bone marrow derived from at least three wild-type and *Igf2-P2* mutant mice. (**B**) Number of giant TRAP$^+$ osteoclasts obtained ex vivo from bone marrow-derived from at least three wild-type and *Igf2-P2* mutant mice. (**C**) Representative pictures of bone marrow-derived wild-type and *Igf2-P2* mutant osteoclasts. (**D**) Numbers of giant, medium-sized and mononucleated TRAP$^+$ osteoclasts obtained ex vivo from spleens derived from at least three wild-type and *Igf2-P2* mutant mice. (**E**) Number of giant TRAP$^+$ osteoclasts obtained ex vivo from spleen derived from at least three wild-type and *Igf2-P2* mutant mice. (**F**) Representative pictures of TRAP$^+$ osteoclasts obtained ex vivo from wild-type and *Igf2-P2* mutant cells. (**G**) Real-time PCR analysis of mRNA levels of transcription factor PPARγ, receptor activator of NF-κB ligand (RANKL) and osteoprotegerin (OPG), a decoy receptor for RANKL, in femurs of 3- to 4-month-old *Igf2-P2* mutant mice relative to wild type. *Igf2-P2* PPARγ, RANKL and OPG mRNA levels are shown as percentages of wild-type PPARγ, RANKL and OPG mRNA levels. Results are the mean ± s.e.m. of results obtained from three *Igf2-P2* mutant and three wild-type mice, with 10^5 cells/well of a 96-well plate. Each sample was analyzed by q-PCR in triplicate and normalized to β-actin mRNA levels (PPARγ and RANKL; $P<0.005$).

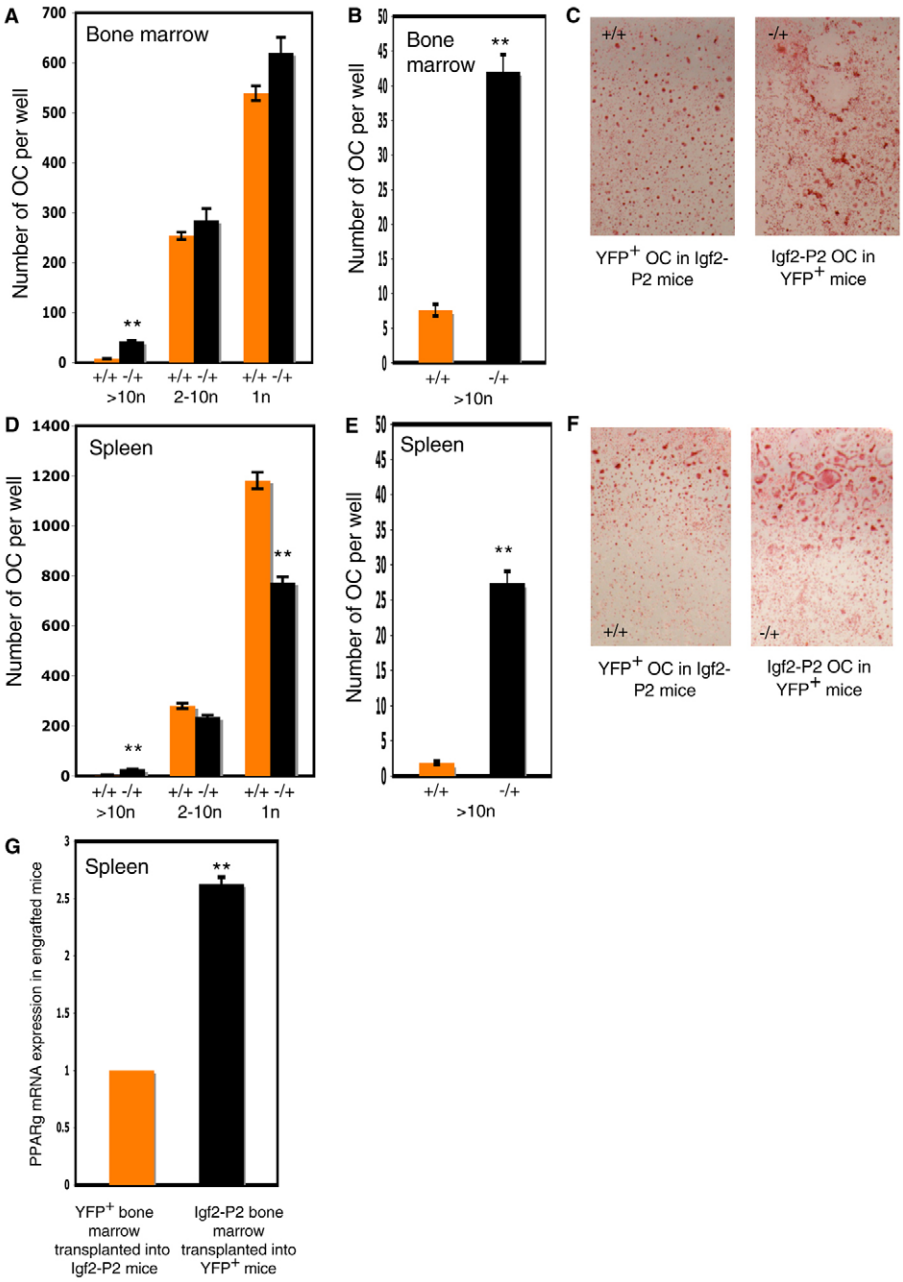

Fig. 5. *Igf2-P2* micro-environment regulates the formation of giant osteoclasts. (**A**) Numbers of giant, medium-sized and mononucleated TRAP$^+$ osteoclasts obtained ex vivo from three mice transplanted with bone marrow-derived wild-type YFP$^+$ (orange columns) and *Igf2-P2* mutant (black columns) cells. (**B**) Number of giant TRAP$^+$ osteoclasts obtained ex vivo from three mice transplanted with bone marrow from wild-type YFP$^+$ and *Igf2-P2* mutant cells. (**C**) Representative pictures of bone marrow-derived giant TRAP$^+$ osteoclasts from transplanted wild-type YFP$^+$ or *Igf2-P2* mutant cells. (**D**) Numbers of giant, medium-sized and mononucleated TRAP$^+$ osteoclasts obtained ex vivo from spleen-derived wild-type YFP$^+$ and *Igf2-P2* mutant cells. (**E**) Number of giant TRAP$^+$ osteoclasts obtained ex vivo from spleen-derived wild-type YFP$^+$ and *Igf2-P2* mutant cells. (**F**) Representative pictures of TRAP$^+$ osteoclasts obtained ex vivo from wild-type YFP$^+$ and *Igf2-P2* mutant mice. (**G**) Fold increase in PPARγ mRNA level in spleens from 3- to 4-month-old YFP$^+$ mice transplanted with *Igf2-P2* deficient bone marrow. PPARγ mRNA levels in spleens of YFP$^+$ mice transplanted with *Igf2-P2* mutant bone marrow are expressed relative to PPARγ mRNA levels in spleens of *Igf2-P2* mutant mice transplanted with YFP$^+$ bone marrow. Values are mean±s.e.m. of three mice. q-PCR was carried out in triplicate and normalized to β-actin mRNA levels (**P<0.005).

the defective osteoclastogenesis in vivo is a secondary effect of a primary stromal defect. Furthermore, the number of giant osteoclasts that developed was decreased when mutant osteoblasts or mutant spleen cells were used, demonstrating that there was an intrinsic defect in osteoclast maturation in mutant mice (Fig. 6B). Similar results were obtained with spleens from 3- and 10-month-old mice, indicating that the osteoclast phenotype did not improve in older *Igf2-P2* mutant mice. The decreased number of giant osteoclasts in *Igf2-P2* mutant mice may therefore limit the severity of the osteoblastic defect of these mice.

DISCUSSION

Transcription of the *Igf2* gene primarily determines IGF2 production and, as a consequence, many developmental features. The *Igf2* gene has four promoters that are conserved between human and mouse, and, until now, few studies have been performed to decipher the precise roles of the different transcriptional units of the *Igf2* gene in vivo. The complete lack of IGF2 in *Igf2*-null mice triggers a permanent 40% growth deficiency (DeChiara et al., 1990), whereas the lack of the placental P0 promoter makes *Igf2-P0* mice 30% smaller at birth owing to a lack of nutrients transport, but mutant mice can catch up in growth during the first 3 months of postnatal life (Constância et al., 2002). As the *Igf2-P2* transcriptional unit has the broadest expression during embryogenesis, is highly expressed in tumor cells and can be detected in some adult progenitors (Vorwerk et al., 2003; Morison et al., 2000), we inactivated the P2-initiated transcription unit by homologous recombination in order to determine whether it was playing a specific role in immature cells. Mice deficient in *Igf2-P2* transcripts had continuous growth retardation leading to harmonious dwarfism reminiscent of, but different from, that associated with the *Igf2* gene inactivation. The

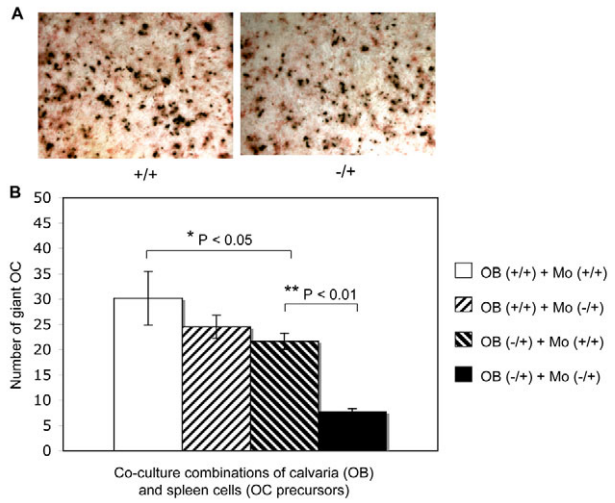

Fig. 6. The *Igf2-P2* mutant mice also have a cell-autonomous osteoclast defect. (**A**) Osteoblastic differentiation of calvaria cells from wild-type (+/+, left panel) and *Igf2-P2* mutant (–/+, right panel) newborn mice. (**B**) Wild-type cells (OB +/+) or *Igf2-P2* mutant cells (OB –/+) from newborns calvaria co-cultured with wild-type or mutant spleen cells (Mo, monocytes). Numbers of giant osteoclasts obtained in all culture combinations from three wild-type and three *Igf2-P2* mutant mice in each experiment (*n*=3).

two mutations led to growth retardation at birth but their adult phenotypes were different and there was a major temporal difference in the way these two phenotypes developed during embryogenesis. In *Igf2*-null embryos, the precipitous drop in body weight to 70% of the wild type that occurs between E10.5 and E11.5 (Baker et al., 1993) has been shown to be due primarily to a modification of cell survival and proliferation (Burns and Hassan, 2001), whereas *Igf2-P2* mutant embryos of the same age manifested only a relatively mild, although significant, growth retardation, reaching the final 30% growth deficit around E16.5. This growth curve might reflect two specific roles for the *Igf2-P2* transcripts. During organogenesis, i.e. before E13.5, *Igf2-P2* transcripts might be crucial for the establishment of discrete founder cell populations, in particular stem/progenitor cells that are present or arise before E10.5 and that are necessary to establish organs. After E13.5, and given that the second part of gestation is dedicated mostly to cell proliferation, *Igf2-P2* transcripts might be required for promotion of fast cell proliferation that would explain the 30% growth deficit observed from E16.5 in *Igf2-P2* mutant fetuses.

Although, in mouse, postnatal skeletal growth is commonly attributed to growth hormone and IGF1 (Karsenty et al., 2009; Kawai and Rosen, 2009; Giustina et al., 2008), since IGF2 is thought to act only during development, the skeletal abnormalities observed in the *Igf2-P2* mice prompted us to study the role of IGF2 in skeletogenesis. During skeletal development, *Igf2-P2* transcripts regulated the pool of embryonic chondroprogenitors, of bone marrow MSCs (CFU-f) and of early transit-amplifying osteoprogenitors. In the adult, *Igf2-P2* transcripts were involved in all steps of bone formation, establishing and maintaining progenitor cells, modulating their differentiation, acting on bone-forming cells as well as on bone-resorbing osteoclasts and modulating their crosstalk with the environment. The downregulation of RUNX2 and OSX in femoral cells and/or MSC and/or CFU-ALP lacking *Igf2-P2* transcripts suggested that, in mice, transcripts initiated at the *Igf2-P2* promoter may act as inducing factors that act upstream of these two crucial transcription factors of the osteoblast lineage. As Notch and bFGF signaling also regulate osteoblast growth and differentiation by acting on RUNX2 and OSX (Engin et al., 2008; Hilton et al., 2008), interplay between the IGF2 pathway and the Notch and bFGF pathways might regulate the formation of osteoblasts in adults. The lack of catch up growth in adult *Igf2-P2* mutant mice might thus be a consequence of the absence of *Igf2-P2* transcripts in discrete adult stem/progenitor cell populations that might not be detectable using conventional total cell population techniques. We showed that the OPN mRNA level was completely dependent on IGF2 signaling during differentiation of MSCs into CFU-ALP. Establishing the link between IGF2 signaling and OPN is of major interest, as these two molecules are strongly involved in many physiological processes, such as proliferation, cell survival, cell migration and tissue remodeling (Suzuki et al., 2002; Bellahcène et al., 2008), and also in many pathological processes, such as dissemination of cancer cells, in particular breast or prostate cancer cells (Wai and Kuo, 2008), which are highly IGF-dependent and form metastasis preferentially in the bone (Kimura et al., 2010). OPN secreted by osteoblasts has also been shown to be a hematopoietic stem cell niche component (Stier et al., 2005).

The phenotype of *Igf2-P2* mutant osteoclasts was associated with decreased mRNA levels of PPARγ, which has been shown to regulate osteoclast differentiation and to trigger osteopetrosis when inactivated (Wan et al., 2007). Impaired osteoclastogenesis was partly due to an impaired interaction with mutant osteoblasts and to a cell-autonomous defect. Interestingly, bone marrow transplantation showed that the reversion of the osteoclast phenotype, which is associated with a partial rescue of PPARγ mRNA levels, required a wild-type micro-environment and revealed that *Igf2-P2* transcripts modulated the terminal differentiation of osteoclasts essentially by a stroma-driven effect. This effect might be linked to the decreased expression of OPN in osteoblasts and bone marrow of *Igf2-P2* mutant mice, as cell-autonomous expression of OPN by monocytes/macrophages is required for monocytes-macrophages fusion during osteoclastogenesis (Chellaiah et al., 2003) and as stromal expression of OPN by osteoblasts is necessary for a proper induction of osteoclastogenesis. Furthermore, in the spleen, where OPN is weakly expressed, a reproducible decrease in mononucleated osteoclasts was observed even after mutant bone marrow was engrafted into a wild-type micro-environment, strengthening the conclusion of a role of OPN in the terminal differentiation of monocytes-macrophages into osteoclasts.

Bone has the potential for regeneration during adult life through osteogenesis, a mechanism that recapitulates many of the events occurring during embryonic development. In particular, it has been shown that osteogenesis is strongly dependant on adhesion processes, involving matrix components such as type I collagen and OPN, as well as members of the integrin family, all required for the adhesion, migration, proliferation and differentiation of osteoblasts (Hidalgo-Bastida et al., 2010). Moreover, the involvement of specific integrins in the activation of the osteoblast-specific transcription factor RUNX2 has been demonstrated (Xiao et al., 1998). Such molecules might be involved in the phenotype and behavior of *Igf2-P2* mutant osteoblasts and osteoclasts, and are currently under investigation. *Igf2-P2* transcripts would thus modulate osteogenesis by limiting the number of stem/progenitors and their interactions with the environment.

The bone micro-environment is crucial to sustain and balance stem cell activity and tissue homeostasis throughout the lifetime of the organism (Sackstein et al., 2008). As a consequence, bone has become a major target for regenerative medicine and cancer therapies but relatively little is known about the mechanisms that control MSC and osteoprogenitor self-renewal and commitment or about the crosstalk between osteoblasts, osteoclasts and cancer metastasis. This study showed that *Igf2-P2* transcripts act in a cell autonomous and non-autonomous manner to regulate the pool of stem/progenitors and of stromal components that are crucial for proper differentiation of osteoblasts and osteoclasts and for bone homeostasis. It pinpointed the *Igf2-P2* mutant mice as a new model with which to study the dynamic interaction between the MSC or the hematopoietic cells and their stromal environment.

Acknowledgements
We are grateful to Marina Gertsenstein and the TCP (Toronto Center for Phenogenomics) transgenic core facility (www.phenogenomics.ca/transgenics/services.html); to the Animal core facility at TCP, to the Samuel Lunenfeld Research Institute's CMHD mouse physiology facility (www.cmhd.ca) and to the CMHD pathology facility at TCP for their technical screening services; and to the Bone Interface Group at the Institute of Biomaterials and Biomedical Engineering of Toronto University for the micro CT analyses. S.N.H. thanks Dr A. Efstratiadis for the *Igf2*-null mice and acknowledges B. Segovia for excellent technical help with the western blotting experiments. This work was supported by INSERM (S.N.H., P.H.R.), STI (Stem Cell Inc grant to A.N.) and operating grants from the Canadian Institutes of Health Research (FRN 83704 to J.E.A.).

Competing interests statement
The authors declare no competing financial interests.

Author contributions
S.N.H. conceived the project, designed, performed and interpreted the experiments, and wrote the paper; R.G. performed bone cell cultures; A.N. provided new tools; P.H.R. and J.E.A. discussed the results and edited the paper.

Supplementary material
Supplementary material for this article is available at
http://dev.biologists.org/lookup/suppl/doi:10.1242/dev.054916/-/DC1

References
Baker, J., Liu, J. P., Robertson, E. J. and Efstratiadis, A. (1993). Role of insulin-like growth factors in embryonic and postnatal growth. *Cell* **75**, 73-82.
Belfiore, A., Frasca, F., Pandini, G., Sciacca, L. and Vigneri, R. (2009). Insulin receptor isoforms and insulin receptor/insulin-like growth factor receptor hybrids in physiology and disease. *Endocrinol. Rev.* **30**, 586-623.
Bellahcène, A., Castronovo, V., Ogbureke, K. U., Fisher, L. W. and Fedarko, N. S. (2008). Small integrin-binding ligand N-linked glycoproteins (SIBLINGs): multifunctional proteins in cancer. *Nat. Rev. Cancer* **8**, 212-226.
Blahovec, J., Kostecka, Z., Lacroix, M. C., Cabanie, L., Godeau, F., Mester, J. and Cavaille, F. (2001). Mitogenic activity of high molecular weight forms of insulin-like growth factor-II in amniotic fluid. *J. Endocrinol.* **169**, 563-572.
Burns, J. L. and Hassan, A. B. (2001). Cell survival and proliferation are modified by insulin-like growth factor 2 between days 9 and 10 of mouse gestation. *Development* **128**, 3819-3830.
Chellaiah, M. A., Kizer, N., Biswas, R., Alvarez, U., Strauss-Schoenberger, J., Rifas, L., Rittling, S. R., Denhardt, D. T. and Hruska, K. A. (2003). Osteopontin deficiency produces osteoclast dysfunction due to reduced CD44 surface expression. *Mol. Biol. Cell* **14**, 173-189.
Conlon, I. and Raff, M. (1999). Size control in animal development. *Cell* **96**, 235-244.
Constância, M., Hemberger, M., Hughes, J., Dean, W., Ferguson-Smith, A., Fundele, R., Stewart, F., Kelsey, G., Fowden, A., Sibley, C. and Reik, W. (2002). Placental-specific IGF-II is a major modulator of placental and fetal growth. *Nature* **417**, 945-948.
Cui, H. (2007). Loss of imprinting of IGF2 as an epigenetic marker for the risk of human cancer. *Dis. Markers* **23**, 105-112.
DeChiara, T. M., Efstratiadis, A. and Robertson, E. J. (1990). A growth-deficiency phenotype in heterozygous mice carrying an insulin-like growth factor II gene disrupted by targeting. *Nature* **345**, 78-80.
DeChiara, T. M., Robertson, E. J. and Efstratiadis, A. (1991). Parental imprinting of the mouse insulin-like growth factor II gene. *Cell* **64**, 849-859.
Engin, F., Yao, Z., Yang, T., Zhou, G., Bertin, T., Jiang, M. M., Chen, Y., Wang, L., Zheng, H., Sutton, R. E. et al. (2008). Dimorphic effects of Notch signaling in bone homeostasis. *Nat. Med.* **14**, 299-305.
Federici, M., Porzio, O., Zucaro, L., Fusco, A., Borboni, P., Lauro, D. and Sesti, G. (1997). Distribution of insulin/insulin-like growth factor-I hybrid receptors in human tissues. *Mol. Cell. Endocrinol.* **129**, 121-126.
Gicquel, C., Rossignol, S., Cabrol, S., Houang, M., Steunou, V., Barbu, V., Danton, F., Thibaud, N., Le Merrer, M., Burglen, L. et al. (2005). Epimutation of the telomeric imprinting center region on chromosome 11p15 in Silver-Russell syndrome. *Nat. Genet.* **37**, 1003-1007.
Giustina, A., Mazziotti, G. and Canalis, E. (2008). Growth hormone, insulin-like growth factors and the skeleton. *Endocrinol. Rev.* **29**, 535-559.
Hattori, H., Matsuzaki, A., Suminoe, A., Ihara, K., Eguchi, M., Tajiri, T., Suita, S., Ishii, E. and Hara, T. (2000). Genomic imprinting of insulin-like growth factor-2 in infant leukemia and childhood neuroblastoma. *Cancer* **88**, 2372-2377.
Hidalgo-Bastida, L. A. and Cartmell, S. H. (2010). Mesenchymal stem cells, osteoblasts and extracellular matrix proteins: enhancing cell adhesion and differentiation for bone tissue engeneering. *Tissue Eng. Part B* **16**, 405-412.
Hilton, M. J., Tu, X., Wu, X., Bai, S., Zhao, H., Kobayashi, T., Kronenberg, H. M., Teitelbaum, S. L., Ross, F. P., Kopan, R. and Long, F. (2008). Notch signaling maintains bone marrow mesenchymal progenitors by suppressing osteoblast differentiation. *Nat. Med.* **14**, 306-314.
Hofmann, W. K., Takeuchi, S., Frantzen, M. A., Hoelzer, D. and Koeffler, H. P. (2002). Loss of genomic imprinting of insulin-like growth factor 2 is strongly associated with cellular proliferation in normal hematopoietic cells. *Exp. Hematol.* **30**, 318-323.
Karsenty, G., Kronenberg, H. M. and Settembre, C. (2009). Genetic control of bone formation. *Annu. Rev. Cell Dev. Biol.* **25**, 629-648.
Kawai, M. and Rosen, C. J. (2009). Insulin-like growth factor-I and bone: lessons from mice and men. *Pediatr. Nephrol.* **24**, 1277-1285.
Kimura, T., Kuwata, T., Ashimine, S., Yamazaki, M., Yamauchi, C., Nagai, K., Ikehara, A., Feng, Y., Dimitrov, D. S., Saito, S. and Ochiai, A. (2010). Targeting of bone-derived insulin-like growth factor-II by a human neutralizing antibody suppresses the growth of prostate cancer cells in a human bone environment. *Clin. Cancer Res.* **16**, 121-129.
Lee, J. E., Pintar, J. and Efstratiadis, A. (1990). Pattern of the insulin-like growth factor II gene expression during early mouse embryogenesis. *Development* **110**, 151-159.
Liaw, L., Skinner, M. P., Raines, E. W., Ross, R., Cheresh, D. A., Schwartz, S. M. and Giachelli, C. M. (1995). The adhesive and migratory effects of osteopontin are mediated via distinct cell surface integrins: role of alpha v beta 3 in smooth muscle cell migration to osteopontin in vitro. *J. Clin. Invest.* **95**, 713-724.
Malaval, L., Wade-Guéye, N. M., Boudiffa, M., Fei, J., Zirngibl, R., Chen, F., Laroche, N., Roux, J. P., Burt-Pichat, B., Duboeuf, F. et al. (2008). Bone sialoprotein plays a functional role in bone formation and osteoclastogenesis. *J. Exp. Med.* **205**, 1145-1153.
Morison, I. M., Eccles, M. R. and Reeve, A. M. (2000). Imprinting of insulin-like growth factor 2 is modulated during hematopoiesis. *Blood* **96**, 3023-3028.
Nagy, A., Rossant, J., Nagy, R., Abramov-Newerly, W. and Roder, J. C. (1993). Derivation of completely cell culture-derived mice from early-passage embryonic stem cells. *Proc. Natl. Acad. Sci. USA* **90**, 8424-8428.
Nishio, Y., Dong, Y., Paris, M., O'Keefe, R. J., Schwarz, E. M. and Drissi, H. (2006). Runx2-mediated regulation of the zinc finger Osterix/Sp7 gene. *Gene* **372**, 62-70.
Ping, A. J., Reeve, A. E., Law, D. J., Young, M. R., Boehnke, M. and Feinberg, A. P. (1989). Genetic linkage of Beckwith-Wiedemann syndrome to 11p15. *Am. J. Hum. Genet.* **44**, 720-723.
Randhawa, G. S., Cui, H., Barletta, J. A., Strichman-Almashanu, L. Z., Talpaz, M., Kantarjian, H., Deisseroth, A. B., Champlin, R. C. and Feinberg, A. P. (1998). Loss of imprinting in disease progression in chronic myelogenous leukemia. *Blood* **91**, 3144-3147.
Sackstein, R., Merzaban, J. S., Cain, D. W., Dagia, N. M., Spencer, J. A., Lin, C. P. and Wohlgemuth, R. (2008). *Ex vivo* glycan engineering of CD44 programs human multipotent mesenchymal stromal cell trafficking to bone. *Nat. Med.* **14**, 181-187.
Stier, S., Ko, Y., Forkert, R., Lutz, C., Neuhaus, T., Grunewald, E., Cheng, T., Dombroski, D., Calvi, L. M., Rittling, S. R. and Scadden, D. T. (2005). Osteopontin is a hematopoietic stem cell niche component that negatively regulates stem cell pool size. *J. Exp. Med.* **201**, 1781-1791.
Stylianopoulou, F., Efstratiadis, A., Herbert, J. and Pintar, J. (1988). Pattern of the insulin-like growth factor II gene expression during rat embryogenesis. *Development* **103**, 497-506.
Suzuki, K., Zhu, B., Rittling, S. R., Denhardt, D. T., Goldberg, H. A., McCulloch, C. A. and Sodek, J. (2002). Colocalization of intracellular osteopontin with CD44 is associated with migration, cell fusion, and resorption in osteoclasts. *J. Bone Miner. Res.* **17**, 1486-1497.
Valenzano, K. J., Heath-Monnig, E., Tollefsen, S. E., Lake, M. and Lobel, P. (1998). Biophysical and biological properties of naturally occurring high

molecular weight insulin-like growth factor II variants. *J. Biol. Chem.* **272**, 4804-4813.
Vorwerk, P., Wex, H., Bessert, C., Hohmann, B., Schmidt, U. and Mittler, U. (2003). Loss of imprinting of IGF-II gene in children with acute lymphoblastic leukemia. *Leuk. Res.* **27**, 807-812.
Wai, P. Y. and Kuo, P. C. (2008). Osteopontin: regulation in tumor metastasis. *Cancer Metastasis Rev.* **27**, 103-118.
Wan, Y., Chong, L. W. and Evans, R. M. (2007). PPAR-gamma regulates osteoclastogenesis in mice. *Nat. Med.* **13**, 1496-1503.
Weinkove, D. and Leevers, S. J. (2000). The genetic control of organ growth: insights from Drosophila. *Curr. Opin. Genet. Dev.* **10**, 75-80.
Xiao, G., Wang, D., Benson, M. D., Karsenty, G. and Franceschi, R. T. (1998). *Activation of the Osf2* transcription factor. *J. Biol. Chem.* **273**, 32988-32994.

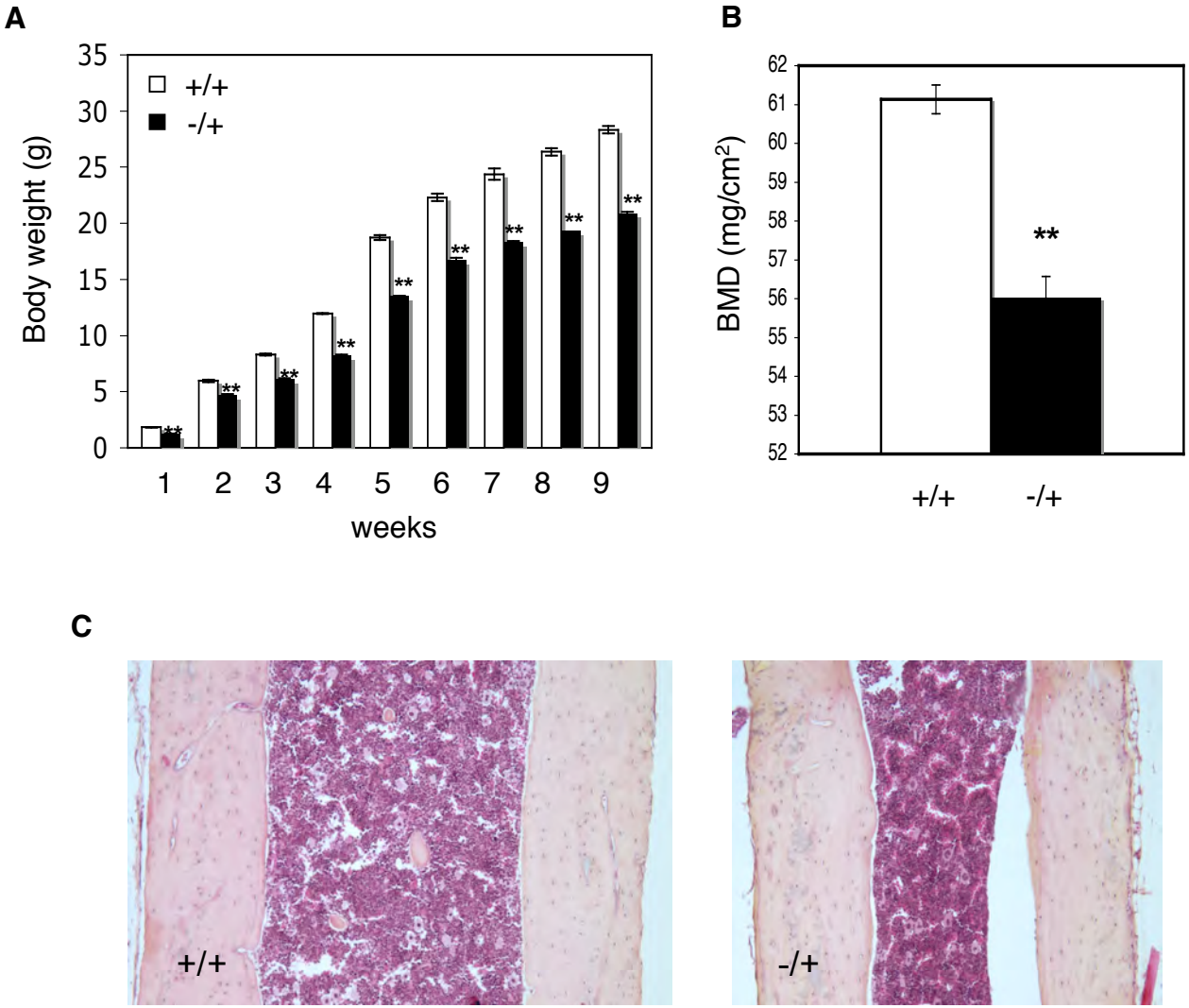
A
Body weight (g)
35
30
25
20
15
10
5
0
+/+
-/+
**
1
2
3
4
5
6
7
8
9
weeks
B
BMD (mg/cm2)
62
61
60
59
58
57
56
55
54
53
52
**
+/+
-/+
C
+/+
-/+

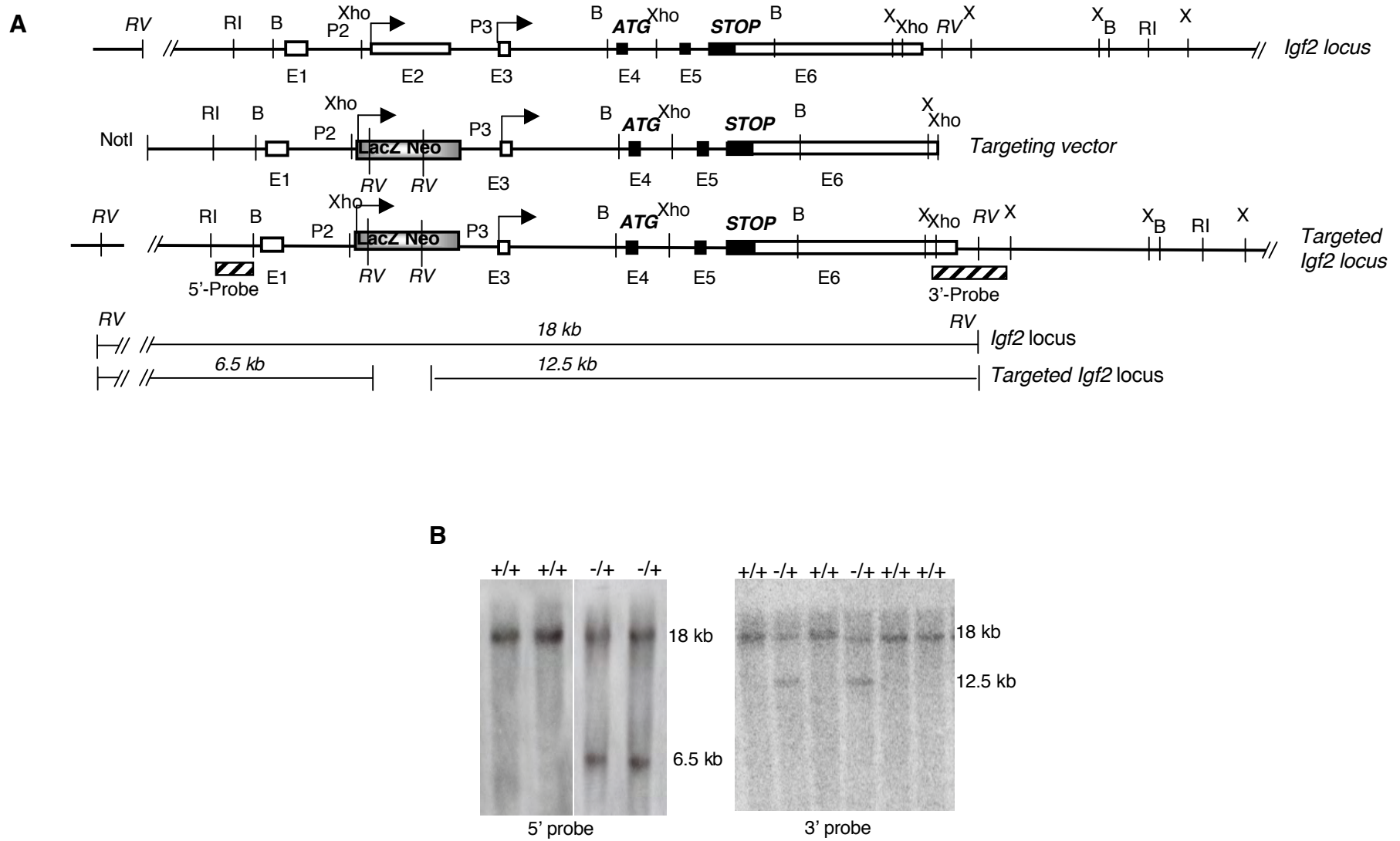
A
RV
RI
B
Xho
P2
P3
ATG
STOP
X
E1
E2
E3
E4
E5
E6
Igf2 locus
NotI
LacZ Neo
Targeting vector
5'-Probe
3'-Probe
Targeted Igf2 locus
18 kb
6.5 kb
12.5 kb
Igf2 locus
Targeted Igf2 locus
B
+/+ +/+ -/+ -/+
+/+ -/+ +/+ -/+ +/+ +/+
18 kb
6.5 kb
12.5 kb
5' probe
3' probe

Table S1. Primers sequences designed for q-PCR analyses

Gene	Sequence	Accession Number	Product size (bp)
Igf2-all	F- TCAGTTTGTCTGTTCGGACCG	U71085	164
	R- TAGACACGTCCCTCTCGGACTT		
Igf2-P3	F- TCCAGCCTTTTCCTGTCTTCA	U71085	96
	R- AAGCACCAACATCGACTTCCC		
β-Actin	F- TCGTGCGTGACATCAAAGAGA	NM007393	144
	R- GAACCGCTCGTTGCCAATA		
Runx2	F- TGTTCTCTGATCGCCTCAGTG	NM009820	173
	R- CCTGGGATCTGTAATCTGACTCT		
Osx	F- ATGGCGTCCTCTCTGCTTG	NM130458	156
	R- TGAAAGGTCAGCGTATGGCTT		
PPARγ	F- TCGCTGATGCACTGCCTATG	NM011146	103
	R- GAGAGGTCCACAGAGCTGATT		
BSP	F- CAGGGAGGCAGTGACTCTTC	NM008318	151
	R- AGTGTGGAAAGTGTGGCGTT		
Opn	F- AGCAAGAAACTCTTCCAAGCAA	NM009263	134
	R- GTGAGATTCGTCAGATTCATCCG		
RANKL	F- CCAGCTATGATGGAAGGCTCA	AB032771	223
	R- CGTACAGGTAATAGAAGCCA		
OPG	F- GGGCGTTACCTGGAGATCG	NM008764	125
	R- GAGAAGAACCCATCTGGACATTT		
ALP	F- CCAACTCTTTTGTGCCAGAGA	NM007431	110
	R- GGCTACATTGGTGTTGAGCTTT		
Col1	F- GCTCCTCTTAGGGGCCACT	NM007742	103
	R- CCACGTCTCACCATTGGG		

The sequences were obtained using Primer Express 2.0 (Perkin Elmer) and the length of the PCR products is indicated.